nature communications

Article

https://doi.org/10.1038/s41467-025-60026-7

Fe-phosphates in Jezero Crater as evidence for an ancient habitable environment on Mars

Received: 10 October 2024

Accepted: 8 May 2025

Published online: 14 July 2025

Check for updates

A list of authors and their affiliations appears at the end of the paper

Phosphorus is an essential component for life, and in-situ identification of phosphate minerals that formed in aqueous conditions directly contributes toward one of the main goals of the Mars 2020 *Perseverance* rover: to seek signs of ancient habitable environments. In Jezero crater, proximity science analyses within a conglomerate outcrop, "*Onahu*" demonstrate the presence of rare Fe^{3+}-bearing phosphate minerals (likely metavivianite, ferrolaueite, (ferro)beraunite, and/or santabarbaraite) embedded in a carbonate-rich matrix. While Fe-phosphates have been inferred previously on Mars, this work presents the most definitive in-situ identification of martian Fe-phosphate minerals to date, using textural, chemical, spectral, and diffraction analyses of discrete green-blue grains. The Fe-phosphate minerals' textural context along with comparisons to Earth analogs suggest they likely formed after oxidation of Fe^{2+}-phosphate vivianite, the most common Fe-phosphate in sedimentary environments on Earth, often associated with microbial activity and organics. While there is no obvious evidence of biological inputs in *Onahu*, if the Fe-phosphates' formation environment was similar to vivianite-rich sedimentary environments on Earth, these minerals likely originally precipitated in conditions favorable to potential martian life — in a low temperature, reducing aqueous medium with high concentrations of bio-limiting elements, and Fe-redox gradients that could provide an energy source. If the sample collected from *Onahu* (*Otis_Peak*) is returned to Earth, analysis of the Fe-phosphates may provide new insights into ancient habitable environments on Mars.

On February 18, 2021 the Mars 2020 rover *Perseverance* landed on the floor of Jezero crater, a ~45 km diameter impact crater that once contained a lake[1]. The crater hosts an ancient, well-preserved depositional fan/delta complex composed of sediments transported and deposited by streams >3.2-3.8 billion years ago[2–8]. Detailed investigation of the sediments and rocks in the Jezero fan can thus provide insights into the physical and chemical conditions in ancient aqueous environments on Mars, the duration and nature of past habitable environments, and their potential to sustain biological or prebiotic processes.

At the time of this writing, *Perseverance* has collected 11 samples from the fan for potential return to Earth, all currently stowed within the rover's Sample and Caching System (like the sample we discuss here) or cached at the Three Forks Sample Depot. Here, we report the detailed mineralogical and chemical analysis of a conglomerate outcrop, informally named *Onahu*, sampled by *Perseverance* on Mars solar day (Sol) 882 (sample name *Otis_Peak*). *Onahu* is located on the top of Jezero's western fan and provides the most definitive in-situ identification of Fe-phosphate minerals on Mars, observed as large (~100 s µm wide) green-blue grains (Fig. 1A).

e-mail: tkizovski@brocku.ca

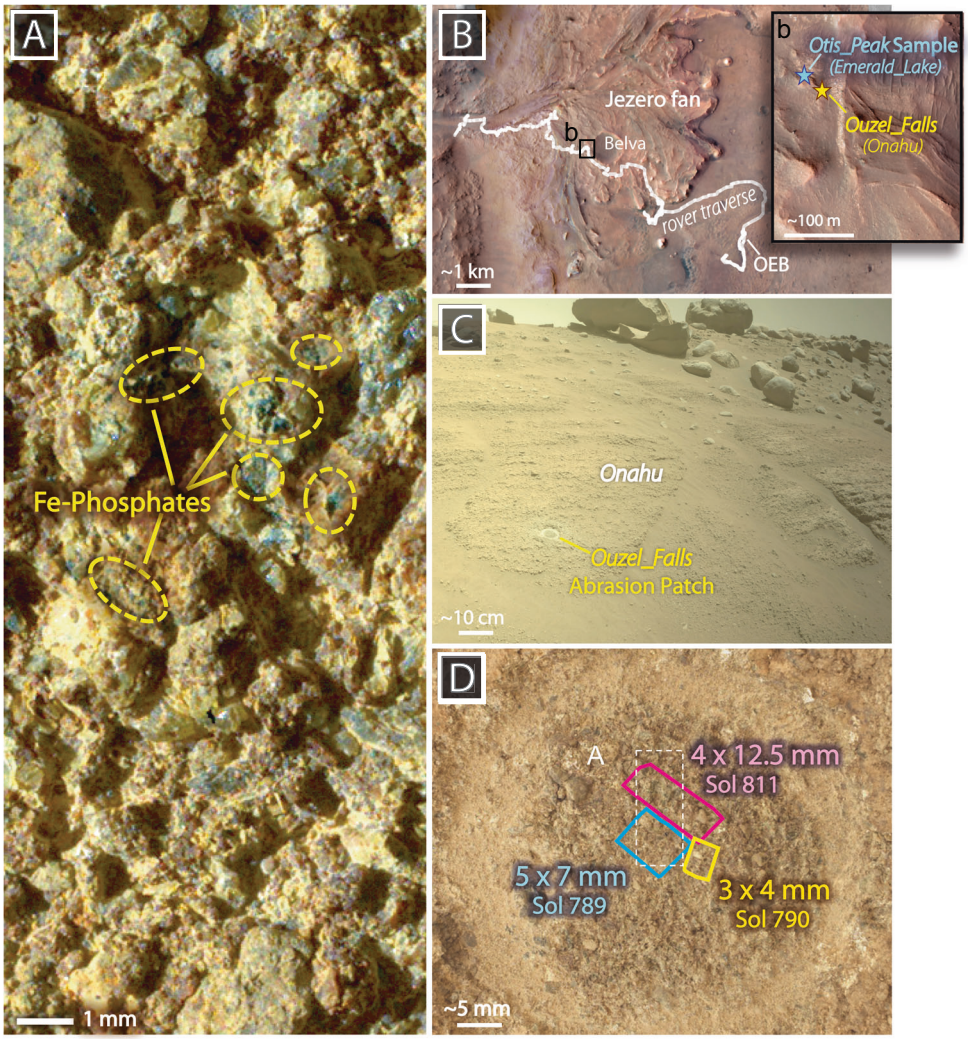

Fig. 1 | Context images for the Fe-phosphates in *Onahu*, and the Ouzel_Falls abrasion patch. A WATSON image enhanced color and with 1% contrast stretch showing the location of the green-blue Fe-phosphate minerals in the *Ouzel_Falls* abrasion patch on the *Onahu* outcrop. **B** HiRISE (High Resolution Imaging Science Experiment) image of Jezero crater showing the traverse path of *Perseverance* up to ~1000 Sols on Mars (OEB = Octavia E. Butler Landing Site). Inset (b) HiRISE image showing the location of the *Onahu* outcrop where PIXL analysis was conducted, and the *Emerald_Lake* workspace where a correlative sample was collected. **C** Front HazCam image of the *Ouzel_Falls* abrasion patch on the pebbly conglomerate outcrop *Onahu*. (D) WATSON image of the *Ouzel_Falls* abrasion patch with PIXL footprints outlined. Mars 2020 image reference numbers are provided in Table S1.

Fe-phosphate minerals are rare on Earth and Mars, where Ca-phosphates are the dominant phosphate minerals (i.e., fluorapatite on Earth, and merrillite and chlorapatite on Mars[9]). Fe-phosphates have been inferred on Mars before in Gale and Gusev crater[9–11], but, until now, have never been directly observed on the surface as we show here, using a combination of high-resolution imaging, chemical, and micro-structural analysis. Phosphate minerals are high value targets for Mars sample return because their chemistry and textural occurrence can be used to constrain the bioavailability of P for prebiotic chemical reactions and/or potential life[9], past aqueous conditions on Mars[9,12,13]; and when igneous in origin, insights into magmatic volatile abundances[14–16]. Fe-phosphate minerals that precipitate in aqueous environments are particularly important astrobiological targets as they have been observed on Earth as products of dissimilatory Fe-reducing bacteria[17,18], encrusting bacterial cells[19], and growing on the hydroxyapatite components of bones, shells, and fossils that have reacted with Fe-rich fluids[17,20]. While biotic influences are not essential for Fe-phosphate formation on Earth or Mars, terrestrial Fe-phosphates are commonly associated with organic matter, either growing on or replacing plant detritus, or precipitating in environments where degradation of organic debris results in more reducing and P-rich conditions[17].

This work summarizes the detailed textural, chemical, reflectance, and micro-structural diffraction analysis of the *Onahu* Fe-phosphates using the Planetary Instrument for X-ray Lithochemistry (PIXL) – a mapping X-ray fluorescence spectrometer[21] – and images from the Scanning Habitable Environments with Raman and Luminescence for Organics and Chemicals (SHERLOC) instrument[22], both mounted on the arm of the rover. The high-resolution PIXL and SHERLOC results are used to identify the Fe-phosphate mineral that is most likely present in *Onahu*, constrain the paleoenvironmental conditions that led to their formation, and assess if these conditions were habitable.

Results And Discussion

Imaging and compositional analyses of *Onahu*

Onahu is in the *Otis_Peak* formation (fm), recognized by its fluvial deposits of planar laminated and cross-stratified sandstone to granule conglomerates. Large, scattered boulders (called the 'rubbly unit') overlie the *Otis_Peak* fm, which could have been sourced from the olivine-rich units common outside Jezero crater[23–25]. The laminated,

poorly sorted medium-grained sandstones of the *Skrinkle_Haven* member (*Tenby* fm) lie beneath the *Otis_Peak* fm[23].

The Fe-phosphates described here were identified in a 50 mm circular abrasion patch informally named *Ouzel_Falls* abraded into the pebbly, cross-stratified conglomerate *Onahu* that crops out on the top of the western Jezero fan (Fig. 1B,C). The outcrop's surface was abraded to remove surface dust and coatings and to provide a relatively smooth surface for analyses by proximity science instruments (PIXL and SHERLOC).

This work focuses on X-ray fluorescence (XRF) maps (3 maps collected between Sols 789–811; Fig. 1D), X-ray diffraction analysis of individual Fe-phosphate grains, and reflectance spectral images collected by PIXL, as SHERLOC Raman spectroscopy maps did not include the Fe-phosphate-rich areas. However, microscopic images collected by SHERLOC cameras (color Wide Angle Topographic Sensor for Operations and eNgineering [WATSON] images with ~15.9 μm/pixel resolution) provide complementary high-resolution context images of the *Ouzel_Falls* abrasion patch.

Chemistry

PIXL maps show the *Ouzel_Falls* abrasion patch is predominantly composed of gravel- to pebble-sized clasts of olivine (Fo_{61}), altered mafic clasts with elevated Fe+Mg/Si (potentially basaltic polymineralic clasts that have been altered to clay minerals), and relatively Mg-rich Mg-Fe-carbonates (Mg# ~55) embedded in a fine-grained matrix. The matrix includes domains rich in Si and Mg-Fe-sulfate, and domains rich in relatively Fe-rich Fe-Mg-carbonate (Mg# ~31), intermixed with fine-grained fragments of the major clast types (Fig. 2A-C, Supplementary Figs. S4-S7, and Tables S3,S4).

Fe-phosphates were identified in the carbonate-bearing matrix domain by their high P and Fe concentrations (up to 24.7 wt% P_2O_5 and 48.8 wt% FeO). These Fe-P "hot-spots" are closely correlated with the ~50–500 μm green-blue grains visible in WATSON images (Figs. 1A, 2B). Because the green-blue grains are similar to or smaller than the PIXL beam size, all the Fe-P-rich PMCs (PIXL Motion Counters = integers corresponding to each analysis point location in a PIXL map) contain elements that are present in surrounding minerals (e.g., Si and S) and are interpreted as mixtures of Fe-phosphate and surrounding matrix material. This mixing relationship is clear in Fig. 2D, which shows that the Fe-P hot-spots are consistent with mixtures of Fe-phosphate minerals and the major phases in *Ouzel_Falls*. Simulated models of these mixtures also produce trends similar to the empirical PIXL data presented here (see Supplementary Information and Figures S2,S3).

At PIXL's resolution, the Fe-phosphates appear to be predominantly composed of only Fe and P based on the strong compositional and spatial correlation between the two elements (Fig. 2B,E). There are no other obvious correlations between high-P concentrations and other cations that are commonly found in phosphate minerals such as Ca, Al, Mg, Mn, and Na (Supplementary Fig. S1). No trace elements except Ni were detected in the Fe-phosphate-bearing PMCs (Supplementary Table S2).

Based on the lack of correlation with other major and trace elements, the composition of the Fe-phosphates is estimated here by determining the P/Fe ratio of the PMCs that contain the most Fe-phosphate (PMCs with $P_2O_5 > 10$ wt%, $SiO_2 < 30$ wt%, $SO_3 < 5$ wt%). The slope of a weighted orthogonal regression through these points (a weighted linear regression that accounts for errors in both x and y variables carried out using the scipy.odr package in Python[26,27]) indicates the Fe-phosphates have P/Fe molar ratios of approximately 0.67 ± 0.11 (~2/3; Fig. 2E). The non-zero intercept from this regression (0.14±0.05) is consistent with mixing with surrounding Fe-bearing phases. According to our literature review and the RRUFF database of International Mineralogical Association approved minerals[28], 19 known terrestrial Fe-phosphate minerals have P/Fe ratios in this range (see Supplementary Table S5). It should be noted however that the P/Fe ratio determined here is a first order estimate based on discretionary SiO_2, P_2O_5, and SO_3 thresholds (Figure S1), and there is likely more unquantified uncertainty as the Fe-phosphates are mixed with multiple end-members which is difficult to model with a linear correlation trend.

Minor phases identified by PIXL in the *Ouzel_Falls* abrasion include sulfates and spinels. The bulk composition of *Ouzel_Falls* contains significant sulfur (~6.6 wt% SO_3; Table S2), most of which can be ascribed to Mg-Fe-sulfate minerals. Areas enriched in Mg and S were found across the PIXL scans, and typically associated with the Si-rich matrix (Supplementary Fig. S6). Ca-sulfate is uncommon in *Ouzel_Falls* and occurs in discrete monomineralic areas. Small grains of Cr-Ti spinel (likely Ti-bearing chromite) are rare and randomly distributed (Supplementary Fig. S8).

Reflectance

To identify which Fe-phosphate mineral with P/Fe ~2/3 is most likely present in *Ouzel_Falls* we examined their reflectance spectra in more detail using PIXL's Micro Context Camera (MCC). The Fe-phosphates can be readily delineated using Green/Near Infrared (G/NIR) band ratio images, standing out as regions with the highest G/NIR in the abrasion patch (Fig. 3A-C).

Four of the grains with the highest P concentrations were selected for further analysis and comparison with terrestrial Fe-phosphate reflectance spectra mainly compiled by the RELAB database[29]. We focus on reflectance ratios baselined with the NIR band, as this band is dominant in discerning the grains from the matrix. The available bands of PIXL's MCC are; ultraviolet [UV, 385 nm], green [G; 530 nm], blue [B, 450 nm], and near-infrared [NIR, 735 nm]. As such, detailed comparisons between PIXL spectral profiles which contain only 4 bands, and high resolution RELAB measurements are limited. Moreover, there is additional uncertainty due to particle size effects on the spectral profiles, as RELAB measurements are based on powdered material.

The Fe-phosphate grains in *Ouzel_Falls* have distinct UV/NIR and G/NIR (Fig. 3D). The average reflectance ratios of Grains 1-3 are relatively similar, varying between 0.91-0.94 G/NIR and 0.60-0.71 UV/NIR, while Grain 4's averages are much lower with 0.79 G/NIR, and 0.46 UV/NIR, revealing an overall increase in NIR relative to other wavelengths in this grain and possibly a different Fe-phosphate phase. Furthermore, many of the individual pixels within Grains 1–3 have similar reflectance ratios to the more ferrous terrestrial Fe-phosphates (vivianite and metavivianite), while the individual pixels from the core of Grain 4 are more similar to terrestrial ferric phosphates (strunzite and strengite).

Only the cores of each grain were used for comparison to terrestrial Fe-phosphates in Fig. 3D in order to minimize any mixing with surrounding *Ouzel_Falls* matrix. In order to assess if any zoning is present, additional analysis of the cores and rims of each grain were carried out (Supplementary Materials and Figures S9-S16, Table S6). The G/NIR ratio of Grains 1–3 were noted to decrease from grain core to rim, either indicative of mixing between the green-blue phosphates with surrounding reddish matrix, and/or possible zoning between green cores and redder rims within the phosphates themselves. Grain 4 is again unique, with very similar G/NIR ratios from core to rim, and a very slight increase in G/NIR from core to rim – opposite to the trend observed in Grains 1–3. The relatively low G/NIR signature from the core of Grain 4 could be due to the presence of a redder Fe-phosphate phase in the core vs rim, or insufficient abrasion as this grain is slightly recessed relative to the other grains within the abrasion patch.

In summary, based on the reflectance ratios of individual pixels within each grain (Fig. 3D), the Fe-phosphates reflectance spectra in *Ouzel_Falls* likely represent mixtures of relatively ferrous phosphates and more oxidized phosphates with higher NIR reflectance, and/or mixtures with the high NIR matrix that surrounds each grain at *Ouzel_Falls*. However, the significantly higher NIR reflectance in Grain 4

https://doi.org/10.1038/s41467-025-60026-7

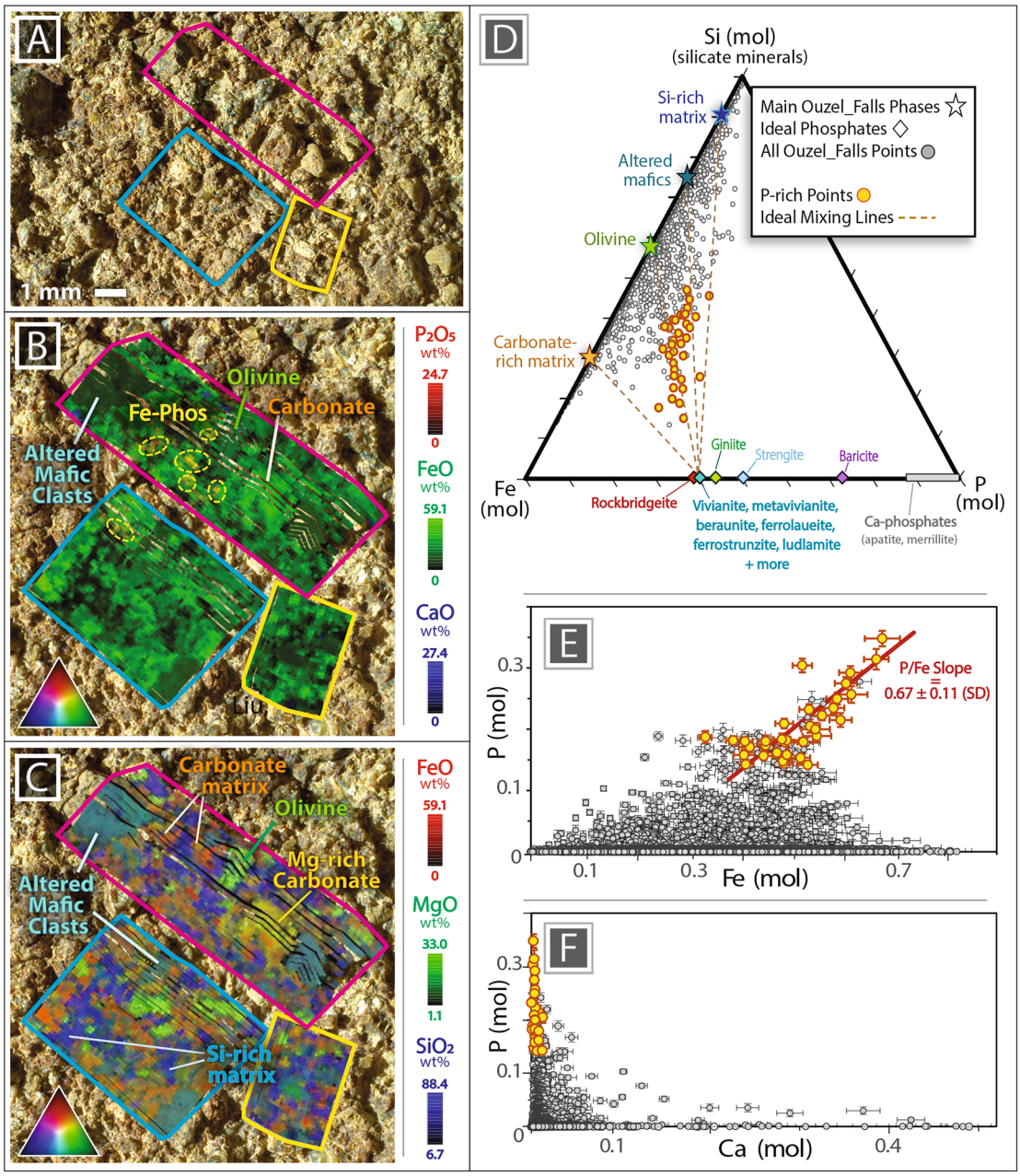

Fig. 2 | Compositional and textural analyzes of *Ouzel_Falls* by PIXL and WATSON. WATSON image with enhanced color and 1% contrast stretch (**A**) and PIXL Red-Green Blue (RGB) X-Ray-Fluorescence (XRF) maps (**B**, **C**) showing the location of the green-blue Fe-phosphate minerals, and other major phases in the *Ouzel_Falls* abrasion patch. RGB triangles show how color mixing between elements will appear, i.e., Fe+P = yellow in (**B**). The approximate footprints of the PIXL scans are shown in (**A**–**C**). **D** Ternary diagram illustrating compositional mixing between *Ouzel_Falls* silicates, carbonates, and Fe-phosphates at PIXL's resolution with ideal linear mixing trends between the major phases and an Fe-phosphate with a P/Fe ratio of ~2/3. The high-P PMCs (PIXL Motion Counters) include those with $P_2O_5 > 10$ wt%, $SiO_2 < 30$ wt%, and $SO_3 < 5$ wt%. Terrestrial Fe-phosphate minerals compositions compiled from ideal stoichiometry. (**E**, **F**) PIXL XRF data illustrating how high-P PMCs are correlated with high-Fe concentrations and decorrelated with Ca. A weighted orthogonal regression through the high-P points in (**E**) results in a P/Fe slope ratio of 0.67 ± 0.11 (SD = Standard Deviation) (P/Fe ~2/3), b = −0.14 ±0.05. All quantitative element concentrations are corrected for surface roughness and diffraction using the method outlined in ref.[38] (Supplementary Dataset 1).

in comparison to Grains 1–3 could indicate it is a separate, more oxidized phase (Fig. 3D). The decrease in G/NIR and UV/NIR as oxidation increases in Fe-phosphates has also been observed in experimentally oxidized synthetic vivianite[30].

Bright regions in the G/NIR images are also associated with vitreous olivine grains, and as such, estimating the volume of Fe-phosphates across the abrasion patch using MCC imaging is ambiguous. If the PIXL scan areas are assumed to be representative of the entire rock, *Onahu* contains ~1 vol% Fe-phosphates (78 PMCs > 10 wt% P_2O_5 / 6495 PMCs total).

Crystal Structure

As terrestrial reflectance data from Fe-phosphates are limited, further analysis is needed to narrow down the most likely Fe-phosphate phase(s) at *Ouzel_Falls*. Here we use X-ray diffraction peaks detected by PIXL to assess the Fe-phosphates' crystallinity and compare their respective diffraction patterns to terrestrial Fe-phosphates. X-ray diffraction peaks in the *Ouzel_Falls* Fe-P hotspots indicate that the Fe-phosphates are predominantly crystalline, i.e., with grain sizes larger than >30–50 µm in the region with diffraction peaks (Fig. 4, and Supplementary Information). Diffraction peaks were also detected

https://doi.org/10.1038/s41467-025-60026-7

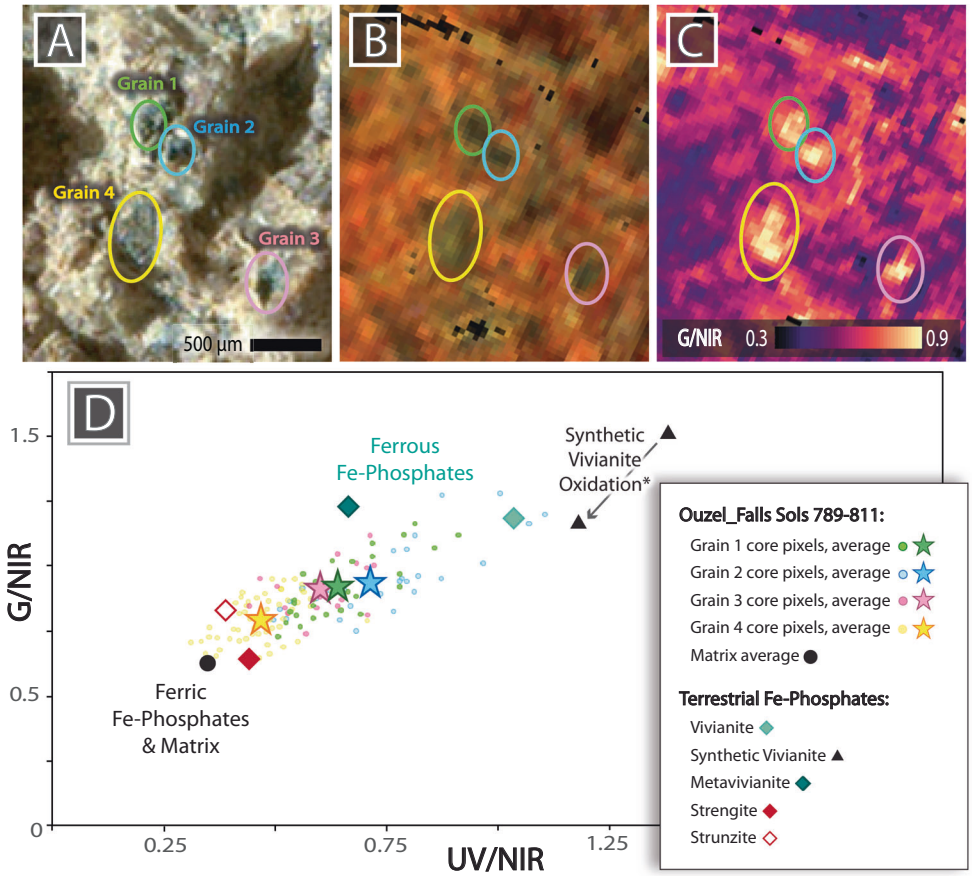

Fig. 3 | PIXL MCC (Micro Context Camera) reflectance analysis of the *Onahu* Fe-phosphates. A WATSON image of the Fe-phosphates within the *Ouzel_Falls* abrasion patch with no enhancement so colors are more comparable to PIXL MCC. **B** PIXL MCC false color RGB image, **C** PIXL MCC Green/Near Infrared (G/NIR) image. Fe-phosphate grains are circled in each image, with 4 representative grains selected for reflectance spectra comparison. **D** Binary plot showing the variation in UV/NIR and G/NIR in the *Ouzel_Falls* abrasion patch. The *Ouzel_Falls* Fe-phosphate grains plot in between terrestrial ferrous and ferric phosphates and surrounding matrix indicating they are likely mixtures at PIXL's MCC resolution. Compilation of reflectance spectra for terrestrial phosphate minerals (sourced from the RELAB database[29] [samples: vivianite specimen JB-JLB-G65, strunzite specimen JB-JLB-B99-B, strengite specimen JB-JLB-742], University of Winnipeg for metavivianite [collected using methods from[75]], and[30] for synthetic vivianite* subjected to 1 minute of oxidation vs. 23 hours of oxidation.

from the olivine and carbonate. The clays and high-Si matrix regions either do not diffract or diffract poorly, indicating they are either amorphous or micro-crystalline with grain sizes <30–50 µm[31].

From the 19 Fe-phosphate minerals with P/Fe ratios ~2/3 (Supplementary Tables S5, S7), 10 were selected for diffraction pattern comparison with the *Ouzel_Falls* Fe-phosphates in order to identify the most likely phase(s). The 10 phosphates were selected either based on their similarity to the *Ouzel_Falls* phosphates in color and reflectance, their prevalence on Earth and Mars, and/or as compositional end-members for completeness, and include:

- Vivianite [$Fe^{2+}_3(PO_4)_2{\cdot}8H_2O$] – often blue/green in color with similar reflectance band ratios to some of the *Ouzel_Falls* Fe-phosphates, the most common Fe-phosphate in sedimentary environments on Earth[17].
- Metavivianite [$Fe^{2+}Fe^{3+}_2(PO_4)_2(OH)_2{\cdot}6H_2O$]– often dark blue/green to black in color with similar reflectance band ratios to some of the *Ouzel_Falls* Fe-phosphates, and an oxidation product of vivianite[30].
- Beraunite [$Fe^{3+}_6(PO_4)_4O(OH)_4{\cdot}6H_2O$] – often red to red-brown, a ferric end-member for comparison.
- Ferroberaunite [$Fe^{2+}Fe^{3+}_5(PO_4)_4(OH)_5{\cdot}6H_2O$] – often green to brown or gray, and a more reduced form of beraunite.
- Strengite [$Fe^{3+}PO_4{\cdot}2H_2O$] – occurs in a variety of colors, compositionally unlikely (i.e., molar P/Fe ratio of 1:1), but reflectance is relatively similar to some of the *Ouzel_Falls* Fe-phosphates, and previously inferred to occur on Mars in the Paso Robles soils, Gusev Crater[11].
- Rockbridgeite [$(Fe^{2+}_{0.5}Fe^{3+}_{0.5})_2Fe^{3+}_3(PO_4)_3(OH)_5$] – often blue/green in color, and an Fe-rich end-member.
- Sarcopside [$Fe^{2+}_3(PO_4)_2$] – occurs in a variety of colors, and an anhydrous end-member for comparison.
- Ferrolaueite [$Fe^{2+}Fe^{3+}_2(PO_4)_2(OH)_2{\cdot}8H_2O$] – typically brown to orange-brown, but its Mn-rich end-member laueite [$Mn^{2+}Fe^{3+}_2(PO_4)_2(OH)_2{\cdot}8H_2O$] was recently inferred to be present on Mars as an oxidation product of Mn-rich vivianite at the Groken Site, Gale Crater[10]. Laueite was also included in the diffraction analysis for completeness.
- Ferrostrunzite and Ferristrunzite [$Fe^{3+}\ Fe^{2+}_2(PO_4)_2(OH)_2{\cdot}6H_2O$ and $Fe^{3+}Fe^{2+}_2(PO_4)_2(OH)_3{\cdot}5H_2O$] – typically yellow to light-brown, but their Mn-rich end-member strunzite [$Mn^{2+}Fe^{3+}_2(PO_4)_2(OH)_2{\cdot}6H_2O$] was also recently inferred to be on Mars with laueite as an oxidation product of Mn-rich vivianite at the Groken Site, Gale Crater[10]. Ferristrunzite has also been inferred in P-rich Paso Robles soil, Gusev Crater[11]. Strunzite was also included in the diffraction analysis for completeness and due to its similar reflectance band ratios to some of the *Ouzel_Falls* Fe-phosphates.

Out of the 12 Fe-phosphates listed above (also including laueite and strunzite), the intensity and position of the detected X-ray diffraction peaks are most consistent with metavivianite, beraunite,

https://doi.org/10.1038/s41467-025-60026-7

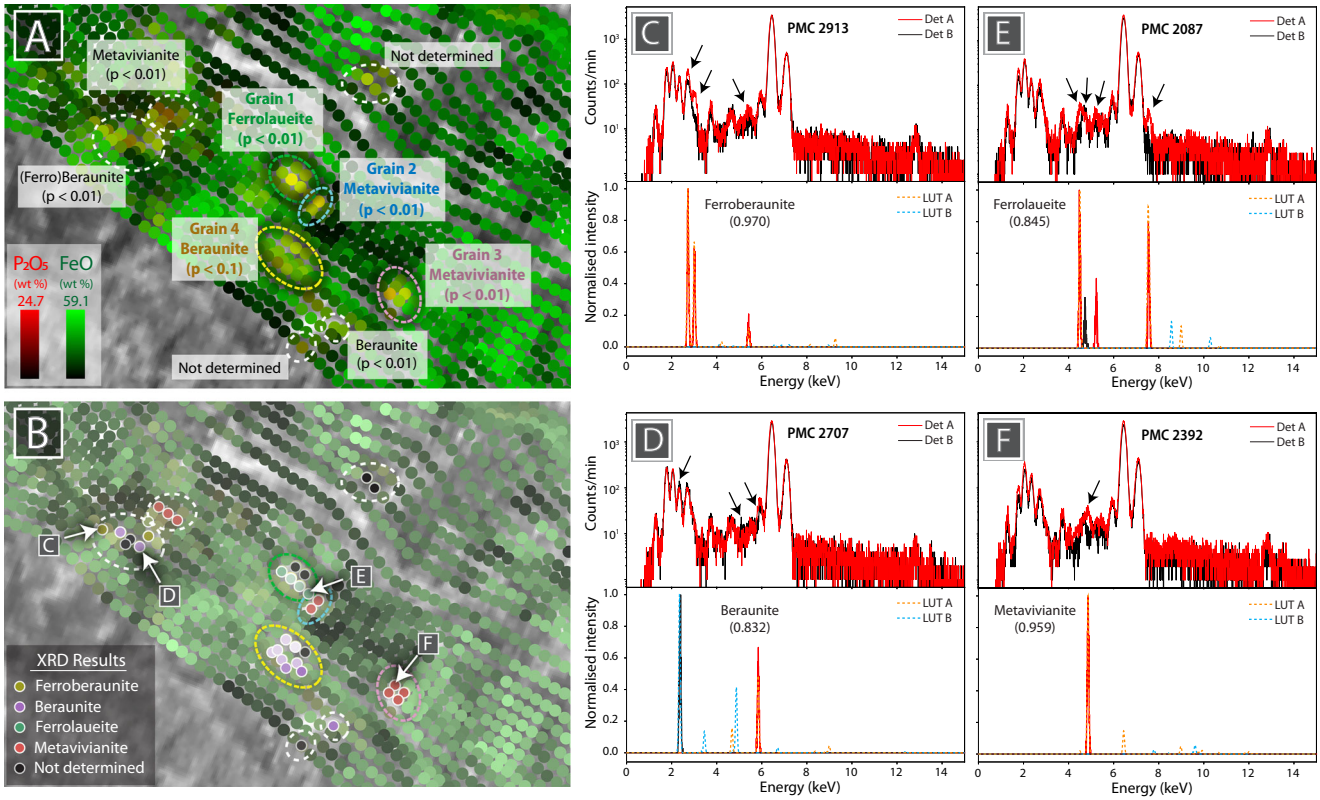

Fig. 4 | Diffraction analysis results. A PIXL X-ray Fluorescence (XRF) map of the *Ouzel_Falls* abrasion patch overlain with the results of the sum diffraction analysis for each high-P region (dashed ovals) shown together with the relevant *p* value for that region. Grains 1-4 were also used for reflectance analysis and are colored in the same scheme as Fig. 3. One region labeled "(Ferro)Beraunite" is likely a combination of ferroberaunite and beraunite. **B** Desaturated PIXL XRF map of the *Ouzel_Falls* abrasion patch overlain with the results of the diffraction analysis per PMC. Circles over the analyzed PMCs are colored according to the identified mineral with the cross-correlation value represented as transparency (min = 0.679, max = 0.979, mean = 0.897). PMCs where the diffraction analysis could not uniquely identify a single Fe-phosphate mineral with high confidence are labeled "Not determined" either as a result of no diffraction detected (i.e., are amorphous to PIXL[31]) or the results of the diffraction analysis were ambiguous and thus no reliable mineral identification could be made. **C**–**F** Examples of spectra from each of PIXLs detectors are shown with the measured diffraction (identified with black arrows where there is a peak in one spectrum and not the other) that is compared to a look up table for all possible diffraction profiles for each together with the cross-correlation between the Look Up Table (LUT) and the measured diffraction (see supplementary material).

ferroberaunite, and/or ferrolaueite (Fig. 4). The results from diffraction analysis are consistent with reflectance spectra for each grain as those with the highest relative NIR reflectance (i.e., Grain 4 Fig. 4D) are identified as Fe^{3+}-rich beraunite, while grains with relatively low NIR reflectance (and higher G/NIR ratios) are identified as mixed valence metavivianite and ferrolaueite (Grains 1–3, Fig. 4E,F).

Fe-Phosphate Identification

Chemical, reflectance, and diffraction analysis of the Fe-phosphates in *Ouzel_Falls* by PIXL indicate that the secondary phosphate minerals metavivianite, (ferro)beraunite, and/or ferrolaueite are likely present. This is the first time these rare Fe-phosphate minerals have been identified on Mars.

These minerals (as well as others of the 19 Fe-phosphate minerals with P/Fe molar ratios ~2/3) can also be differentiated based on their Fe-oxidation state and H_2O contents. While PIXL is unable to directly measure these components, other instruments on the Perseverance Rover are sensitive to hydration and oxidation (SuperCam and SHERLOC). Unfortunately, these instruments did not target the Fe-phosphates in *Ouzel_Falls*.

Metavivianite, beraunite, and ferrolaueite can all form on Earth in association with the Fe-phosphate mineral vivianite[30,32,33]. Vivianite occurs as green-blue crystals and is the most common Fe-phosphate formed in sedimentary environments on Earth[17]. It is also found as a secondary phase in a variety of hydrothermal settings[17]. Metavivianite (triclinic) forms from vivianite (monoclinic) as Fe^{3+} increases, resulting in a degradation of crystal symmetry and darkening in color[34]. If Fe-oxidation continues, eventually the orange-brown amorphous pseudomineral santabarbaraite ($Fe^{3+}{}_3(PO_4)_2(OH)_3{\bullet}5H_2O$) forms after metavivianite[20,30]. Reflectance spectra for santabarbaraite were not available for comparison at this time, however, we hypothesize that mixtures of dark green-blue to black metavivianite and orange-brown santabarbaraite and/or other Fe^{3+}-phosphates could also produce the high NIR reflectance observed in the *Ouzel_Falls* phosphates (Fig. 3D).

Beraunite and ferrolaueite are much less common on Earth than vivianite, but both can occur associated with vivianite as Fe-oxidation products like metavivianite; or conversely be reduced to form vivianite[32,33,35,36]. Ferroberaunite is a relatively new mineral[37], and slightly reduced form of beraunite that has been often misidentified as green beraunite in similar formation environments.

As all of these phases can occur together, it is possible that the Fe-phosphate assemblage at *Ouzel_Falls* comprises a mixture of (ferro) beraunite, metavivianite, ferrolaueite, santabarbaraite, vivianite, and/or other Fe-phosphate minerals that we are not able to differentiate at PIXL's resolution, or where terrestrial analog data needed for comparison are limited. For example, no reflectance spectra for beraunite, ferroberaunite, or ferrolaueite were available for comparison at the time of this writing.

https://doi.org/10.1038/s41467-025-60026-7

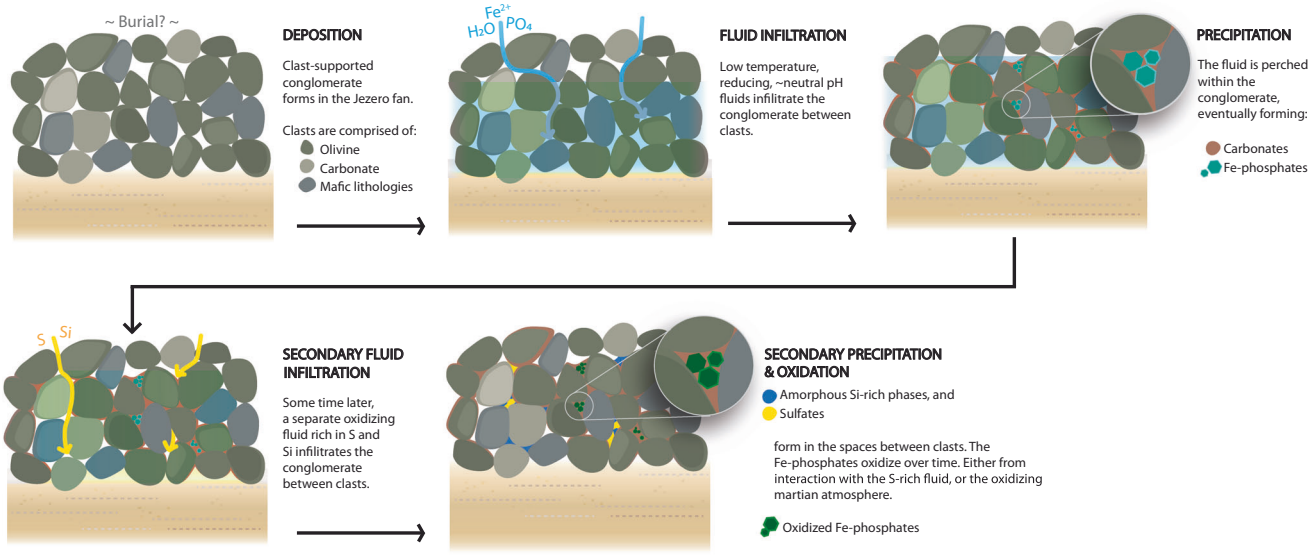

Fig. 5 | Cartoon illustrating the potential paleoenvironmental history of the *Onahu* outcrop and Fe-phosphates if they formed authigenically. Multiple episodes of fluid-rock interactions or evolving fluid compositions are needed to explain the distinct occurrences of carbonate-rich matrix and Si,S-rich matrix. Detrital Fe-phosphates could also have been incorporated into the conglomerate before fluid infiltration.

Fe-Phosphates Origin and Paleoenvironmental Conditions

In order to constrain the paleoenvironmental conditions that led to the formation of the Fe-phosphates in *Ouzel_Falls*, we first need to consider if they were incorporated into the *Onahu* conglomerate as detrital phases, or if they formed in place.

In either case, the Fe-phosphates described here are the first to be identified and sampled by *Perseverance*, indicating a unique formation environment (Ca-phosphates are common in Jezero crater[9,38,39]). Additionally, as metavivianite, ferrolaueite, (ferro)beraunite, and/or santabarbaraite are all known to form after oxidation of vivianite on Earth, it is assumed that they first formed as vivianite in a more reducing environment before being exposed to oxidizing conditions either within the *Onahu* conglomerate itself, or within the Jezero paleolake watershed.

Authigenic origin

The Fe-phosphates occur only in the Fe-Mg-carbonate-rich matrix, suggesting that they might have precipitated in-place (as vivianite), in the pore space of the coarse-grained conglomerate at the same time as the carbonate, or filled the remaining pore space after carbonate precipitation.

Experimental studies have shown that vivianite readily precipitates from aqueous solution in the presence of Fe^{2+} and PO_4^{3-} [40,41]. Because the speciation of aqueous phosphate is strongly dependent on pH, and more aqueous phosphate is converted to PO_4^{3-} at higher pH values, vivianite often forms in natural systems at circumneutral pH (e.g., pH 6–9[17]), and where Fe^{2+} and dissolved phosphate are present[40,41]. In anoxic lakes on Earth, the P/Fe^{2+} ratio needed for authigenic formation is relatively high, typically ~1:6 or more, and >1:30 in laboratory experiments[42]. These conditions may be met in inorganic systems and in biologically influenced systems. For instance, thermodynamic calculations based on new solubility measurements have shown that vivianite may form through the evaporation of dilute surface waters on Mars under anoxic conditions that support ferrous iron[43]. On Earth, vivianite tends to form where dissimilatory microbial reduction of Fe(III)-bearing phases in sedimentary environments increases pH, and releases Fe^{2+} and dissolved phosphate that is commonly bound to Fe(III)-oxide minerals[17]. Fe-rich carbonate, which occurs with the Fe-phosphates in *Onahu*, is also known to precipitate with vivianite on Earth in anoxic zones through the same process when organic carbon oxidation is coupled with reduction of Fe(III)-oxides[17,44]. Still, on an anoxic, less Fe(III)-rich[45,46], and relatively P-rich early Mars[47], similar associations of microbes and iron would not be needed to produce the reducing, Fe^{2+}, and P-rich conditions where vivianite (and carbonate) can precipitate.

Authigenic vivianite formation has been previously inferred on Mars at the Groken Site, Gale Crater (although it was not directly observed) where it may have precipitated in P-Mn-rich nodules[10,48]. The Groken P-Mn-rich nodules are thought to have originally precipitated as Mn-rich vivianite within sediment pore space from a locally P-rich, reduced groundwater[10]. Over time, the vivianite was likely oxidized to laueite and/or strunzite, and eventually to the main components of the nodules today – hematite and Mn-hydroxide[10].

The presence of metavivianite, ferrolaueite, (ferro)beraunite, and/or santabarbaraite in *Ouzel_Falls* suggests that the original vivianite crystals must have also undergone oxidation in-place if authigenic. The formation of separate phosphate-carbonate-rich, and Si-sulfate-rich domains in the conglomerate matrix (Fig. 2C) indicates that diagenesis in *Onahu* occurred under evolving paleoenvironmental conditions and potentially different redox states. It is hypothesized here that the vivianite originally precipitated in a reducing Fe^{2+}-rich fluid associated with the formation of the carbonate-rich matrix (based on their co-occurrence), and was then eventually oxidized either from alteration by infiltrating oxidizing Si-S-rich fluids that formed the Si- and sulfate-rich (oxidized S) matrix in the remaining pore space and/or from exposure to the oxidizing martian atmosphere (Fig. 5). Based on the persistence of carbonate, it is assumed that if a Si- and sulfate-rich fluid infiltrated into the Fe-phosphates-carbonate matrix, the fluid was not strongly acidic, and/or the water-rock interaction was short lived. Regardless, vivianite is also relatively insoluble in low pH environments (in comparison to Ca-phosphates)[9].

The *Ouzel_Falls* abrasion patch is also the most P-enriched PIXL target analyzed within the western fan (Supplementary Fig. S17; Table S2), particularly in comparison to other carbonate-rich siliciclastic rocks, indicating that, if authigenic, the Fe-phosphates likely formed from a localized P-rich fluid.

While the textural occurrence of Fe-phosphates within the Fe-rich carbonate-bearing matrix, the presence of two discrete matrix

domains, and the overall P-enrichment in *Ouzel_Falls* support a model where vivianite precipitated and oxidized in-place, we should also consider if the Fe-phosphates may have precipitated from a similar process in sediments upstream within the Jezero paleolake watershed and were concentrated in the carbonate-rich matrix in *Onahu* through sorting.

Detrital origin

Terrestrial Fe-phosphates are not common detrital phases, and to our knowledge, have never been identified. Vivianite and metavivianite are soft (Mohs hardness of 1.5-2, and 2.5, respectively[17,49]) and unlikely to persist during extended fluvial or eolian transport. Beraunite, ferroberaunite, and ferrolaueite are slightly harder, with Mohs hardness of 3–4[32,37,50].

A source of detrital Fe-phosphates in *Onahu* could be upstream sediments where vivianite formed in a similar process as described above. However, vivianite and its oxidation products are also known to occur on Earth as secondary minerals in altered P-rich pegmatites[36,51,52] or in metal-rich ore bodies (with either igneous or sedimentary protoliths) and skarn deposits[50,53]. At this time, there is no evidence of pegmatites, metal-rich ore bodies, and/or skarn deposits in the Jezero watershed (or elsewhere on Mars), but the discovery of highly evolved Fe-rich basalts on the Jezero crater floor[38,54] indicates that more extreme differentiated lithologies could exist in the watershed that we are not able to identify with remote analyses alone.

The Jezero watershed is also known to contain significantly altered rock based on the presence of smectite, carbonate, and incision of the altered basement and mottled terrain units by fluvial valleys[5]. Aqueous alteration models demonstrate it is possible for Fe-phosphates to form during weathering of Ca-phosphate-bearing ultramafic rocks[55]; as such, they could have originally formed in the Jezero watershed from this process.

Regardless of the inferred origin of the Fe-phosphates, based on our current knowledge of the Jezero watershed, and comparisons to terrestrial environments, the *Onahu* Fe-phosphates most likely are not igneous or hydrothermal in origin and formed in a P- and Fe-rich aqueous environment at relatively low temperatures either as precipitates in sediments or as alteration products of P-rich rocks. If detrital, oxidation of vivianite could have occurred before or after transport and incorporation into *Onahu*.

Implications for habitability and Mars sample return

The identification of secondary Fe-phosphate minerals (metavivianite, ferrolaueite, (ferro)beraunite, and/or santabarbaraite) after vivianite in *Ouzel_Falls* provides evidence that many of the materials and energy source(s) needed for habitable conditions may have existed in the Jezero fan top, and/or within the Jezero paleolake watershed. Vivianite and its oxidation products have been inferred on Mars before[9–11], but this is the first time the Fe-phosphates noted here have been identified using correlative high-resolution chemical, structural, reflectance, and imaging analyses.

Based on comparisons to natural systems on Earth, the vivianite in *Ouzel_Falls* most likely precipitated in conditions favorable to potential martian life within a low temperature, anoxic, reducing aqueous medium at approximately neutral pH[17], with high concentrations of bio-limiting elements including carbon and phosphorus, and Fe-redox gradients that could provide an energy source. For example, dissimilatory reduction of ferric ions by bacteria when phosphorus is available, to the ferrous form in vivianite, can enable access to metabolic energy[56,57]. These conditions are most likely to have occurred when Mars was warmer and wetter, around the time of the Jezero fan formation (> 3.2 Ga[2–8]).

Although vivianite is thought to have been important in the biogeochemical P cycle on early Earth[43,58,59], it is largely absent from the ancient geologic record, possibly due to oxidation/dissolution driven by diagenesis and metamorphism[58]. In contrast, the results presented here, combined with the well-preserved nature of the western fan[8] suggest the *Onahu* outcrop experienced minimal metamorphic alteration following the formation of the fan ca. 3.2 Ga, thus extending the preservational window of vivianite. However, while the available evidence supports a potentially ancient origin for these well-preserved Fe-phosphates, we cannot rule out their formation in another more recent event.

Many of the conditions needed for vivianite formation are also suitable for the preservation of chemical biosignatures, if present[60]. Terrestrial Fe-phosphates have been observed encrusting bacteria, and growing on/replacing organic detritus and the hydroxyapatite components of bones and fossils[17]. Furthermore, authigenic carbonate minerals like those that occur in the *Ouzel_Falls* matrix are particularly conducive to the preservation of chemical and morphological biosignatures, from organic molecules to microbial fossils[61,62].

Perseverance can provide immense amounts of information on martian paleoenvironments through the identification of rare minerals like the Fe-phosphates described here when high-resolution proximity science instruments are deployed. Still, textural, compositional, and isotopic analyses of the returned sample (*Otis_Peak*) will be essential to constrain the ancient environmental conditions, chemical reactions, or even microbial activity that produced these unusual minerals.

Methods

PIXL Analyses

The PIXL instrument produces maps of elemental abundances on martian surface materials using X-ray Fluorescence (XRF). PIXL's focused X-ray beam interacts with the surface in a ~ 120 μm diameter spot size for fluoresced X-rays of 8 keV, and larger diameters for lower energies[21,31,63]. PIXL rasters its focused X-ray beam across a predefined area of interest, and so produces analyses of multiple spots that are correlated with beam positions; from which the PIXLISE software package[64] produces maps of elemental abundances (see[21,31,38,39] for more details on PIXL's operation). PIXL maps can include thousands of individual X-ray fluorescence spectra, each with unique positions recorded as PIXL Motion Counters (PMCs - integers tracking each time PIXL moves on to a new software activity that correspond to locations of each PIXL analysis in a scanned area).

PIXL obtained three XRF raster scans on the *Ouzel_Falls* abrasion patch (Sols 789, 790, and 811) at step sizes of 0.125 mm, for a total scan area of 97 mm^2 (Fig. 1D). Energy-dispersive XRF spectra were acquired for each point for 10 s each (6495 PMCs total), with an additional 30 s of dwell time when PIXL's adaptive sampling algorithm was triggered on rare phases of interest (such as phosphate minerals) in order to improve signal-to-noise ratios at these locations (123 PMCS, e.g.,[65]). PIXL's micro context camera (MCC) also acquired images of the abrasion patch illuminated by ultraviolet (UV, 385 nm), blue (B, 450 nm), green (G, 530 nm) and near-infrared (735 nm) light emitting diodes (LEDs) with a spatial resolution of ~50 μm/pixel. The preflight calibration of the LED-MCC system allows multispectral analysis of these four wavelengths[66,67]. The XRF and MCC data were then analyzed using PIXLISE, allowing for detailed examination of elemental compositions and X-ray spectral characteristics correlated to context images. PIXLISE fully incorporates instrument calibration of optics, geometry, XRF quantification as well as the in-situ conditions of topographic effects and positional drift caused by diurnal thermal environment, enabling accurate correlation between XRF spectra and context images to within 50 microns[68].

Mineral mixing modeling

PIXL's analytical spot size varies between elements because lighter elements fluoresce at lower energies[63]. The beam diameter varies inversely with energy, meaning higher energy X-rays are focused to a smaller diameter. High-energy X-rays excite more high-energy

fluorescence, so the relationship between PIXL's analytical spot size and X-ray energy results in a larger analytical volume for lighter atoms and a correspondingly inflated measured distribution. While these effects are well-characterized and accounted for in a homogenous sample, they become more complex at grain boundaries. Mixing relationships between neighboring mineral grains appear nonlinear, complicating efforts to determine the "unmixed" end-member compositions of mineral phases that are smaller than, or close to, PIXL's spot size (including the Fe-phosphates of interest here). Thus, to constrain the composition of Fe-phosphates, we modeled compositional mixing between the main minerals in *Ouzel_Falls* and various Fe-phosphate endmembers, taking the energy-dependent variation in spot size for different elements into account. See Supplementary Fig. S3 and Supplementary Information.

Crystallographic mapping and diffraction phase matching

PIXL has two detectors, and so can separate anisotropic X-ray diffraction peaks occurring from crystalline materials from isotropic X-ray fluorescence peaks when energies of PIXL's incident radiation happen to be in a diffracting condition with d-spacings and orientations of crystal lattices in the target materials[69]. Diffraction, as well as surface roughness, can result in misestimation of elemental concentrations, as such, all XRF compositions reported here have been corrected for these effects using the method outlined in ref. 38.

When detected, X-ray diffraction can also be used to assess crystallinity, grain size, and grain texture of a target[31,38,39] and to distinguish among minerals with similar elemental compositions[70]. Here, diffraction patterns from the Fe-P-rich areas of the *Ouzel_Falls* abrasion patch were compared to modeled diffraction patterns for several candidate Fe-phosphate minerals to identify the most likely phases (see Supplementary Information).

Sampling

The *Perseverance* rover attempted twice to collect a sample from the *Onahu* outcrop near and on the *Ouzel_Falls* abrasion patch, but the rock was too friable to acquire an intact core. A final sampling attempt was carried out ~30 meters NNW of the *Onahu* outcrop in a workspace informally named *Emerald_Lake*, in the same stratigraphic layer as *Onahu*. The *Otis_Peak* sample core was successfully acquired from this location.

As PIXL was not used to analyze the *Emerald_Lake* workspace, data from the SuperCam, WATSON, and CacheCam instruments on *Perseverance* are used here to confirm its similarity to *Onahu* (see Supplementary Information, Table S8 and Figures S18,S19).

Data availability

As per guidelines of the NASA Mars 2020 mission, all data underlying the study are available in the public domain, and specifically reside in the Planetary Data System (PDS) Geosciences Node. Compositional and spectral data from PIXL used in this study are available in the PDS Geosciences Node at https://doi.org/10.17189/1522645[71]. The processed chemical PIXL data are available in the Supplementary Information. SuperCam chemical data is available in the PDS Geosciences Node at https://doi.org/10.17189/1522646[72]. ACI and WATSON images can be found in the PDS Geosciences Node at https://planetarydata.jpl.nasa.gov/img/data/mars2020/mars2020_imgops/data_aci_imgops/[73] and https://planetarydata.jpl.nasa.gov/img/data/mars2020/mars2020_imgops/data_watson_imgops/[74], respectively.

References

1. Farley, K. A. et al. Mars 2020 Mission Overview. *Space Sci. Rev.* **216**, 142 (2020).
2. Fassett, C. I. & Head, J. W. The timing of martian valley network activity: Constraints from buffered crater counting. *Icarus* **195**, 61–89 (2008).
3. Fassett, C. I. & Head, J. W. Fluvial sedimentary deposits on Mars: Ancient deltas in a crater lake in the Nili Fossae region. *Geophys. Res. Lett.* **32**, 2005GL023456 (2005).
4. Ehlmann, B. L. et al. Clay minerals in delta deposits and organic preservation potential on Mars. *Nat. Geosci.* **1**, 355–358 (2008).
5. Goudge, T. A., Mustard, J. F., Head, J. W., Fassett, C. I. & Wiseman, S. M. Assessing the mineralogy of the watershed and fan deposits of the Jezero crater paleolake system, Mars. *JGR Planets* **120**, 775–808 (2015).
6. Mangold, N. et al. Fluvial regimes, morphometry, and age of Jezero crater paleolake inlet valleys and their exobiological significance for the 2020 rover mission landing site. *Astrobiology* **20**, 994–1013 (2020).
7. Stack, K. M. et al. Sedimentology and stratigraphy of the shenandoah formation, Western Fan, Jezero Crater, Mars. *JGR Planets* **129**, e2023JE008187 (2024).
8. Bosak, T. et al. Astrobiological potential of rocks acquired by the perseverance rover at a sedimentary fan front in Jezero Crater, Mars. *AGU Adv.* **5**, e2024AV001241 (2024).
9. Hausrath, E. M. et al. Phosphates on Mars and their importance as igneous, aqueous, and astrobiological indicators. *Minerals* **14**, 591 (2024).
10. Treiman, A. H. et al. Manganese-iron phosphate nodules at the groken site, Gale Crater, Mars. *Minerals* **13**, 1122 (2023).
11. Lane, M. D. et al. Mineralogy of the Paso Robles soils on Mars. *Am. Mineralogist* **93**, 728–739 (2008).
12. Hurowitz, J. A. et al. In situ and experimental evidence for acidic weathering of rocks and soils on Mars. *J. Geophys. Res.* **111**, 2005JE002515 (2006).
13. Adcock, C. T. & Hausrath, E. M. Weathering profiles in phosphorus-rich rocks at gusev crater, mars, suggest dissolution of phosphate minerals into potentially habitable near-neutral waters. *Astrobiology* **15**, 1060–1075 (2015).
14. Boyce, J. W., Tomlinson, S. M., McCubbin, F. M., Greenwood, J. P. & Treiman, A. H. The lunar apatite paradox. *Science* **344**, 400–402 (2014).
15. McCubbin, F. M. & Ustunisik, G. Experimental investigation of F and Cl partitioning between apatite and Fe-rich basaltic melt at 0 GPa and 950–1050 °C: evidence for steric controls on apatite-melt exchange equilibria in OH-poor apatite. *Am. Mineralogist* **103**, 1455–1467 (2018).
16. McCubbin, F. M. et al. Experimental investigation of F, Cl, and OH partitioning between apatite and Fe-rich basaltic melt at 1.0–1.2 GPa and 950–1000 °C. *Am. Mineralogist* **100**, 1790–1802 (2015).
17. Rothe, M., Kleeberg, A. & Hupfer, M. The occurrence, identification and environmental relevance of vivianite in waterlogged soils and aquatic sediments. *Earth-Sci. Rev.* **158**, 51–64 (2016).
18. Yuan, Q., Wang, S., Wang, X. & Li, N. Biosynthesis of vivianite from microbial extracellular electron transfer and environmental application. *Sci. Total Environ.* **762**, 143076 (2021).
19. Konhauser, K. O., Fyfe, W. S., Schultze-Lam, S., Ferris, F. G. & Beveridge, T. J. Iron phosphate precipitation by epilithic microbial biofilms in Arctic Canada. *Can. J. Earth Sci.* **31**, 1320–1324 (1994).
20. Shen, M., Lu, Z., Xu, Y. & He, X. Vivianite and its oxidation products in mammoth ivory and their implications to the burial process. *ACS Omega* **6**, 22284–22291 (2021).
21. Allwood, A. C. et al. PIXL: Planetary instrument for X-ray lithochemistry. *Space Sci. Rev.* **216**, 134 (2020).
22. Bhartia, R. et al. Perseverance's Scanning Habitable Environments with Raman and Luminescence for Organics and Chemicals (SHERLOC) Investigation. *Space Sci. Rev.* **217**, 58 (2021).
23. K. L. Siebach et al. PIXL analyses of sedimentary rocks in the Mars 2020 Perseverance upper fan. *55th Lunar and Planetary Science Conference* (2024).

24. Hoefen, T. M. et al. Discovery of olivine in the Nili Fossae region of Mars. *Science* **302**, 627–630 (2003).
25. Ody, A. et al. Global investigation of olivine on Mars: insights into crust and mantle compositions. *J. Geophys. Res.: Planets* **118**, 234–262 (2013).
26. Virtanen, P. et al. SciPy 1.0: fundamental algorithms for scientific computing in Python. *Nat. Methods* **17**, 261–272 (2020).
27. Boggs, P. T. & Rogers, J. E. Orthogonal distance regression. *Contemp. Math.* **112**, 186 (1990).
28. Lafuente, B., Downs, R. T., Yang, H. & Stone, N. The power of databases: the RRUFF project. *Highlights Mineral. Crystallogr.* 1–30 (2015). http://rruff.info/ima/.
29. NASA RELAB facility at Brown University Spectral Database. https://sites.brown.edu/relab/relab-spectral-database/.
30. Liu, W., Wang, Z., Bowden, M., Qafoku, O. & Rosso, K. M. Vivianite oxidation is not photocatalyzed. *Geochimica et. Cosmochimica Acta* **373**, 109–121 (2024).
31. Tice, M. M. et al. Alteration history of Séítah formation rocks inferred by PIXL x-ray fluorescence, x-ray diffraction, and multispectral imaging on Mars. *Sci. Adv.* **8**, eabp9084 (2022).
32. Segeler, C. G., Moore, P. B., Dyar, M. D., Leans, F. & Ferraiolo, J. A. Ferrolaueite, a new mineral from Monmouth County, New Jersey, USA. *Austrian J. Mineral.* **16**, 69–76 (2012).
33. Nriagu, J. O. & Dell, C. I. Diagenetic formation of iron phosphates in recent lake sediments. *Am. Mineralogist* **59**, 934–946 (1974).
34. Čermáková, Z. et al. Temperature-related degradation and colour changes of historic paintings containing vivianite. *Spectrochimica Acta Part A: Mol. Biomolecular Spectrosc.* **140**, 101–110 (2015).
35. Moore, P. B. & Kampf, A. R. Beraunite: refinement, comparative crystal chemistry, and selected bond valences. *Zeitschrift für Kristallographie-Crystalline Materials* **201**, 263–281 (1992).
36. Dill, H. G., Melcher, F., Gerdes, A. & Weber, B. The origin and zoning of hypogene and supergene Fe-Mn-Mg-Sc-U-REE phosphate mineralization from the newly discovered trutzhofmuhle aplite, Hagendorf pegmatite province, Germany. *Can. Mineralogist* **46**, 1131–1157 (2008).
37. Tvrdý, J. et al. Ferroberaunite, Fe^{2+} $Fe^{3+}{}_5$ $(PO_4)_4$ $(OH)_5$ ·$6H_2O$, a mixed-valence iron member of the beraunite series, from the Gravel Hill mine, Perranzabuloe, Cornwall, England. *MinMag* **86**, 363–372 (2022).
38. Schmidt, M. E. et al. Diverse and highly differentiated lava suite in Jezero crater, Mars: constraints on intracrustal magmatism revealed by Mars 2020 PIXL. *Sci. Adv.* **11**, eadr2613 (2025).
39. Liu, Y. et al. An olivine cumulate outcrop on the floor of Jezero crater, Mars. *Science* **377**, 1513–1519 (2022).
40. Al-Borno, A. & Tomson, M. B. The temperature dependence of the solubility product constant of vivianite. *Geochimica et. Cosmochimica Acta* **58**, 5373–5378 (1994).
41. Nriagu, J. O. Stability of vivianite and ion-pair formation in the system $Fe_3(PO_4)^{2}$-H_3PO_4-H_3PO_4-H_2O. *Geochimica et. Cosmochimica Acta* **36**, 459–470 (1972).
42. Xiong, Y., Guilbaud, R., Peacock, C. L., Krom, M. D. & Poulton, S. W. Phosphorus controls on the formation of vivianite versus green rust under anoxic conditions. *Geochimica et. Cosmochimica Acta* **351**, 139–151 (2023).
43. Brady, M. P., Tostevin, R. & Tosca, N. J. Marine phosphate availability and the chemical origins of life on Earth. *Nat. Commun.* **13**, 5162 (2022).
44. Fredrickson, J. K. et al. Biogenic iron mineralization accompanying the dissimilatory reduction of hydrous ferric oxide by a groundwater bacterium. *Geochimica et. Cosmochimica Acta* **62**, 3239–3257 (1998).
45. Liu, J., Michalski, J. R., Wang, Z. & Gao, W.-S. Atmospheric oxidation drove climate change on Noachian Mars. *Nat. Commun.* **15**, 5648 (2024).
46. Chemtob, S. M., Nickerson, R. D., Morris, R. V., Agresti, D. G. & Catalano, J. G. Oxidative Alteration of Ferrous Smectites and Implications for the Redox Evolution of Early Mars. *JGR Planets* **122**, 2469–2488 (2017).
47. Taylor, G. J. The bulk composition of Mars. *Geochemistry* **73**, 401–420 (2013).
48. VanBommel, S. J. et al. Elemental composition of manganese- and phosphorus-rich nodules in the Knockfarril Hill member, Gale crater, Mars. *Icarus* **392**, 115372 (2023).
49. Chukanov, N. V. et al. Metavivianite, $Fe^{2+}Fe^{3+}{}_2(PO_4)_2(OH)_2$·$6H_2O$: new data and formula revision. *Mineral. mag.* **76**, 725–741 (2012).
50. Vrtiška, L. et al. Redefinition of beraunite, $Fe^{3+}{}_6(PO_4)_4O(OH)_4$·$6H_2O$, and discreditation of the name eleonorite: a re-investigation of type material from the Hrbek Mine (Czech Republic). *Eur. J. Mineral.* **34**, 223–238 (2022).
51. Baijot, M., Hatert, F., Dal Bo, F. & Philippo, S. Mineralogy and Petrography of Phosphate Mineral Associations from the Jocao Pegmatite, Minas Gerais, Brazil. *Can. Miner.* **52**, 373–397 (2014).
52. Włodek, A., Grochowina, A., Gołębiowska, B. & Pieczka, A. A phosphate-bearing pegmatite from Lutomia and its relationships to other pegmatites of the Góry Sowie Block, southwestern Poland. *Jour. Geosci.* **60**, 45–72 (2015).
53. Bermanec, V., Šćavničar, S. & ZebeC, V. Childrenite and crandallite from the Stari Trg mine (Trepča), Kosovo: new data. *Mineral. Petrol.* **52**, 197–208 (1995).
54. Udry, A. et al. A Mars 2020 *Perseverance* SuperCam Perspective on the Igneous Nature of the Máaz Formation at Jezero Crater and Link With Séítah, Mars. *JGR Planets* **128**, e2022JE007440 (2023).
55. Hao, J., Knoll, A. H., Huang, F., Hazen, R. M. & Daniel, I. Cycling phosphorus on the Archean Earth: Part I. Continental weathering and riverine transport of phosphorus. *Geochimica et. Cosmochimica Acta* **273**, 70–84 (2020).
56. Lu, Y., Liu, H., Feng, W., Xu, Y. & Chen, X. A new and efficient approach for phosphorus recovery from wastewater in the form of vivianite mediated by iron-reducing bacteria. *J. Water Process Eng.* **42**, 102200 (2021).
57. Eshun, L. E., Coker, V. S., Shaw, S. & Lloyd, J. R. Strategies for optimizing biovivianite production using dissimilatory Fe(III)-reducing bacteria. *Environ. Res.* **242**, 117667 (2024).
58. Hao, J. et al. Cycling phosphorus on the Archean Earth: Part II. Phosphorus limitation on primary production in Archean ecosystems. *Geochim. Cosmochim. Acta* **280**, 360–377 (2020).
59. Walton, C. R. et al. Phosphorus availability on the early Earth and the impacts of life. *Nat. Geosci.* **16**, 399–409 (2023).
60. Hays, L. E. et al. Biosignature Preservation and Detection in Mars Analog Environments. *Astrobiology* **17**, 363–400 (2017).
61. Bosak, T., Moore, K. R., Gong, J. & Grotzinger, J. P. Searching for biosignatures in sedimentary rocks from early Earth and Mars. *Nat. Rev. Earth Environ.* **2**, 490–506 (2021).
62. Tarnas, J. D. et al. Characteristics, Origins, and Biosignature Preservation Potential of Carbonate-Bearing Rocks Within and Outside of Jezero Crater. *JGR Planets* **126**, e2021JE006898 (2021).
63. Das, A. et al. Energy dependence of X-ray beam size produced by polycapillary X-ray optics. *X-Ray Spectrom.* **54**, 203–213 (2024).
64. Schurman, D. et al. *PIXELATE: Novel Visualization And Computational Methods For The Analysis Of Astrobiological Spectroscopy Data*. In *Proc. 2019 Astrobiology Science Conference (AGU AbSciCon 2019)* (2019).
65. Lawson, P. R. et al. Adaptive sampling with PIXL on the Mars Perseverance rover. *Icarus* **429**, 116433 (2025).

66. Henneke, J. et al. A radiometric correction method and performance characteristics for PIXL's multispectral analysis using LEDs. *Space Sci. Rev.* **219**, 68 (2023).
67. Klevang, D. A. et al. Pre-flight geometric and optical calibration of the planetary instrument for X-ray lithochemistry (PIXL). *Space Sci. Rev.* **219**, 11 (2023).
68. Klevang, D. A. et al. *Pre- and In-flight Performance of Terrain Relative Navigation on PIXL's Micro Context Camera, M2020*. In *2024 IEEE Aerospace Conference* 1–14 (IEEE, Big Sky, MT, USA, 2024).
69. Wright, A. P., Nemere, P., Galvin, A., Chau, D. H. & Davidoff, S. *Lessons from the Development of an Anomaly Detection Interface on the Mars Perseverance Rover using the ISHMAP Framework*. In *Proc. 28th International Conference on Intelligent User Interfaces* 91–105 (ACM, Sydney NSW Australia, 2023).
70. Jones, M. W. M. et al. In-situ crystallographic mapping constrains sulfate deposition and timing in Jezero crater. *Sci. Adv.* **11**, eadt3048 (2025).
71. Planetary Data System. Mars 2020 PIXL Raw and Processed Data Bundle Online. https://doi.org/10.17189/1522645.
72. Planetary Data System. Mars 2020 SuperCam Bundle Online. https://doi.org/10.17189/1522646.
73. Planetary Data System Imaging Node (ACI). https://planetarydata.jpl.nasa.gov/img/data/mars2020/mars2020_imgops/data_aci_imgops/
74. Planetary Data System Imaging Node (WATSON). https://planetarydata.jpl.nasa.gov/img/data/mars2020/mars2020_imgops/data_watson_imgops/
75. Izawa, M. R. M. et al. Reflectance spectroscopy of ilmenites and related Ti and Ti Fe oxides (200 to 2500 nm): Spectral–compositional–structural relationships. *Icarus* **362**, 114423 (2021).

Acknowledgements

We are grateful to the Mars 2020 Science and Engineering team members who participated in tactical and strategic science operations. We thank Dr. Janice Bishop and Dr. Winnie Liu for validating the terrestrial Fe-phosphates reflectance data used in this paper. This study was funded through the following sources: the Canadian Space Agency (CSA) M2020 Participating Scientist Program grant 21EXPMAPS CSA 2021 (M.E.S and T.V.K.). and 22EXPCOI4 (EC); NASA, Jet Propulsion laboratory, California Institute of Technology 80NMOO18D0004 (A.C.A, Y.L., A.H.T., J.A.H., M.M.T., M.L.C., B.C.C., S.S.); NASA Participating Scientist Program 80NSSC21K0328 (S.J.V., A.L.K., J.R.C.), 80NSSC21K0331 (K.L.S.), and 80NSSC20K0234 (T.B.); the European Research Council (ERC) Consolidator Grant 818602 (A.G.F.); the Natural Sciences and Engineering Research Council of Canada RGPIN-2023-03413 (E.C.); Canadian Space Agency (CSA) M2020 Returned Sample Participating Scientist Program grant 20EXPMARS (N.R.); and the University of Cambridge (N.J.T.).

Author contributions

All authors contributed to this work. All authors conducted portions of PIXL, SHERLOC, or SCAM data collection and processing. T.V.K. compiled and interpreted the PIXL XRF data with the assistance of M.E.S., L.O., A.H.T., M.M.T., S.J.V., A.O.S., and J.A.H. L.O. and T.V.K. developed the mineral mixing model and interpreted the results. M.W.M.J. compiled and interpreted the diffraction phase matching results. N.J.T., D.A.K., P.S.J., E.C., and T.V.K. compiled and interpreted the MCC reflectance results. Figures were produced by T.V.K., M.W.M.J., S.S., and J.M., with assistance from M.E.S., D.A.K., and P.S.J. T.V.K. wrote the main paper with assistance, input, and review from M.E.S., L.O., M.W.M.J., N.J.T, D.A.K., J.A.H., C.T.A., E.M.H., K.L.S., Z.U.W., S.S., F.M.M., M.L.C., Y.L., B.C.C., A.H.T., D.C.C., T.B., B.P.W., A.G.F., N.R.R, J.R.C., A.L.K., A.O.S., P.R.L., L.W., C.H., W.T.E., and A.C.A. Z.U.W. compiled and interpreted SCAM data, and S.S. compiled and interpreted CacheCam comparison data, J.M. compiled and processed WATSON images. All co-authors reviewed and provided comments on the final manuscript.

Competing interests

The authors declare no competing interests.

Additional information

Supplementary information The online version contains supplementary material available at https://doi.org/10.1038/s41467-025-60026-7.

Correspondence and requests for materials should be addressed to T. V. Kizovski.

Peer review information *Nature Communications* thanks Fabio Rodrigues, who co-reviewed with Gabriel Gonçalves Silva; Melissa Lane and Craig Walton for their contribution to the peer review of this work. A peer review file is available.

T. V. Kizovski[1,2] ✉, M. E. Schmidt[1], L. O'Neil[3], M. W. M. Jones[4], N. J. Tosca[5], D. A. Klevang[6], J. A. Hurowitz[7], C. T. Adcock[8], E. M. Hausrath[9], K. L. Siebach[10], Z. U. Wolf[11], S. Sharma[12,13], S. J. VanBommel[14], F. M. McCubbin[15], E. Cloutis[16], M. L. Cable[12], Y. Liu[12], B. C. Clark[17], A. H. Treiman[18], M. M. Tice[3], D. C. Catling[19], J. Maki[12], T. Bosak[20], B. P. Weiss[20], A. G. Fairén[21,22], J. R. Christian[14], A. L. Knight[14],

A. O. Shumway[19], N. R. Randazzo[23], P. S. Jørgensen[6], P. R. Lawson[12], L. Wade[12], C. Heirwegh[12], W. T. Elam[19] & A. C. Allwood[12]

[1]Department of Earth Sciences, Brock University, St. Catharines, ON, Canada. [2]Department of Earth and Space, Royal Ontario Museum, Toronto, ON, Canada. [3]Department of Geology & Geophysics, Texas A&M University, College Station, TX, USA. [4]School of Chemistry and Physics and Central Analytical Research Facility, Queensland University of Technology, Brisbane, QLD, Australia. [5]Department of Earth Sciences, University of Cambridge, Cambridge, UK. [6]Technical University of Denmark, DTU Space, Department of Measurement and Instrumentation, Kongens, Lyngby, Denmark. [7]Department of Geosciences, Stony Brook University, Stony Brook, NY, USA. [8]School of Science, Engineering & Mathematics, College of Southern Nevada, Las Vegas, NV, USA. [9]Department of Geoscience, University of Nevada, Las Vegas, Nevada, USA. [10]Department of Earth, Environmental and Planetary Sciences, Rice University, Houston, TX, USA. [11]Los Alamos National Laboratory, Los Alamos, New Mexico, USA. [12]Jet Propulsion Laboratory, California Institute of Technology, Pasadena, CA, USA. [13]Carnegie Institution for Science, Washington, DC, USA. [14]McDonnell Center for the Space Sciences, Department of Earth, Environmental, and Planetary Sciences, Washington University in St. Louis, St. Louis, MO, USA. [15]NASA Johnson Space Center, Houston, TX, USA. [16]Department of Geography, University of Winnipeg, Manitoba, Canada. [17]Space Science Institute, Boulder, CO, USA. [18]Lunar and Planetary Institute (USRA), Houston, TX, USA. [19]Department of Earth and Space Sciences, University of Washington, Seattle, WA, USA. [20]Department of Earth, Atmospheric, and Planetary Sciences, Massachusetts Institute of Technology, Cambridge, MA, USA. [21]Centro de Astrobiología (CAB), CSIC-INTA, 28850 Madrid, Spain. [22]Department of Astronomy, Cornell University, Ithaca, NY, USA. [23]Department of Earth and Atmospheric Sciences, University of Alberta, Edmonton, AB, Canada. ✉e-mail: tkizovski@brocku.ca